Facile Low-Cost Synthesis of Highly Photocatalitycally Active Zinc Oxide Powders

frontiers in Materials

ORIGINAL RESEARCH
published: 31 March 2022
doi: 10.3389/fmats.2022.869493

Facile Low-Cost Synthesis of Highly Photocatalitycally Active Zinc Oxide Powders

Y. Y. Kedruk[1], G. A. Baigarinova[2], L. V. Gritsenko[1], G. Cicero[3] and Kh. A. Abdullin[2,4]*

[1]Department of General Physics, Satbayev University, Almaty, Kazakhstan, [2]National Nanotechnology Laboratory of Open Type at Al-Farabi Kazakh National University, Almaty, Kazakhstan, [3]Dipartimento di Scienza Applicata e Tecnologia, Politecnico di Torino, Torino, Italy, [4]Department of Solid State Physics and Nonlinear Physics, Almaty, Kazakhstan

The industrial waste can cause significant harm to human health and to the environment. Organic dyes in particular are environmentally dangerous since they may cause the death of aquatic life or contaminate the feed chain. Thus, one of the current research fields consists of the development of an inexpensive and environmentally friendly method to purify wastewater from organic contaminants. Among the others, Zinc oxide (ZnO) is considered one of the most effective photocatalysts for the decomposition of organic pollutants in water. In this work, we developed a highly efficient low-temperature and environmentally safe synthesis method to obtain photocatalytically active nanostructured ZnO by chemical precipitation from a solution. The effect of the technological conditions of synthesis on the photocatalytic properties is considered in detail, the correlation with the morphology, structural, and optical properties of the synthesized ZnO samples is determined. It was found that the maximum photocatalytic activity with respect to the decomposition of the dye rhodamine-B (RhB) is achieved for samples synthesized at NaOH molar concentration from 0.4 to 0.7 M; in this case, the sizes of crystallites along the crystallographic direction 002 reach maximum values of ~42 nm. On the contrary, the sizes of crystallites along the directions 100 and 101 decrease monotonically from 30 to 25 nm with an increase in the molar concentration of NaOH from 0.14 to 1 M.

Keywords: chemical low-cost deposition method, zinc oxide, optical and structural properties, photocatalytic activity, rhodamine-B

OPEN ACCESS

Edited by:
Harry E. Ruda,
University of Toronto, Canada

Reviewed by:
Masoud Salavati-Niasari,
University of Kashan, Iran
Guozhe Sui,
Qiqihar University, China

****Correspondence:***
L. V. Gritsenko
gritsenko_lv@mail.ru

Specialty section:
This article was submitted to Semiconducting Materials and Devices, a section of the journal Frontiers in Materials

Received: *04 February 2022*
Accepted: *11 March 2022*
Published: *31 March 2022*

Citation:
Kedruk YY, Baigarinova GA, Gritsenko LV, Cicero G and Abdullin KA (2022) Facile Low-Cost Synthesis of Highly Photocatalitycally Active Zinc Oxide Powders. Front. Mater. 9:869493. doi: 10.3389/fmats.2022.869493

INTRODUCTION

Most of nowadays industries such as textile, paint, cellulose, plastic, food, and cosmetics industries, as well as agriculture and livestock farming, are responsible for the discharge of harmful chemical organic dyes into rivers and groundwater (Qi et al., 2017; Nguyen and Nguyen, 2020). These chemicals are not biodegradable, lead to environmental pollution, harming both the ecological state of water bodies and human health (Sousa et al., 2018). For this reason, in recent years scientists have been focusing on developing alternative safe physical and chemical methods for removing organic dyes from wastewater (Hodges et al., 2018; Jeon et al., 2018; Mirzaeifard et al., 2020; Ferreira et al., 2021). One of the most promising methods is photocatalysis, a process in which UV light is used to activate the chemical degradation of a substance in the presence of a catalyst which decreases the process activation energy and increases the reaction rate. Wide bandgap semiconductor materials such as TiO_2 (Katal et al., 2020), CuO (Khiavi et al., 2019; Al–Namshah, 2021), Cu_2O (Su et al., 2018), pure and doped ZnO

(EL-Dafrawy et al., 2021; Islam and Azam, 2021; Ramírez et al., 2021; Tasso Guaraldo et al., 2021), In_2O_3 (Shanmuganathan et al., 2021), Fe_2O_3 (Cao et al., 2020; Zhang et al., 2020), and other oxides have proven to behave as excellent photocatalysts. As shown in a recent paper (Liang et al., 2022), the photocatalytic properties of ZnO can be drastically enhanced by doping and forming a porous nanosized structure containing ZnO/CdS heterojunctions. An upscale utilization of these compounds in large-scale wastewater treatment applications calls for the development of an inexpensive and environmentally friendly method for their synthesis.

Zinc oxide (ZnO) is a wide-band gap (3.37 eV) n-type semiconductor with a high exciton binding energy (60 meV) (Huang et al., 2015) and, in its nanostructured form, is actively used as a base material for solar cells (Consonni et al., 2019; Wibowo et al., 2020), photocatalysis (Aljaafari, 2020; Naji et al., 2020), gas sensors (Wang et al., 2020; Kang et al., 2021), optoelectronic (Harun et al., 2017) and photonic devices (Rahman, 2019; Zakria et al., 2019), in rubber and plastic fillers (Shuai et al., 2021). Several synthesis methods have been proposed in the literature to obtain ZnO nanoparticles with controlled morphology, such as precipitation (Adam et al., 2018), pyrolysis (Wallace et al., 2013), hydrothermal (Alshamsi and Hussein, 2018; Mohan et al., 2020) and sol-gel methods (Harun et al., 2017; Haque et al., 2020), thermal evaporation (Hamid et al., 2021), mechanochemical (Otis et al., 2021), and others (Ong et al., 2018).

However, often the synthesis methods proposed for obtaining photocatalysts have significant drawbacks. For example, the flame spray pyrolysis method (Widiyandari et al., 2020) requires special equipment, uses fossil fuels in addition to zinc precursors, and its performance is difficult to scale. The hydrothermal method (Khudiar et al., 2021) uses reactors that withstand high pressures at temperatures above 100°C, the processing time is difficult to reduce due to the limited heating rate of a massive hydrothermal reactor, and the scaling of the method is costly. A number of synthesis methods require complex expensive equipment, for example, the thermal evaporation method (Ahmoum et al., 2021) uses vacuum equipment, the high-intensity mechanochemical grinding (Shu et al., 2021) uses ball mills and high-strength grinding jars and balls to prevent contamination of the target product. Promising synthesis methods of such products, as photocatalysts are only those methods that do not use expensive equipment as well as long technological processes and can be easily scaled up.

An important applied problem is the photocatalytic degradation of dyes such as Rhodamine. Rhodamine-B ($C_{28}H_{31}ClN_2O_3$) is a toxic fluorescent artificial dye widely used in the industry for example, in the production of colored cardboard, paper or for dyeing leather products. Rhodamine-B is one of the most widely used dyes in the textile industry. A significant part of cosmetics, mainly decorative, having reddish tints, is also made using this dye.

In this work, we developed a highly efficient low-temperature environmentally friendly synthesis method of photocatalytically active nanostructured zinc oxide for the photostimulated decomposition of organic dyes, in particular, rhodamine. Zinc oxide was synthesized by precipitation from a solution containing a Zn precursor. The effect of the alkali concentration in the starting solution on the morphology, structural, optical, and photocatalytic properties of the synthesized ZnO samples has been studied. A relationship has been found between the photocatalytic activity with respect to the decomposition of the rhodamine-B (RhB) dye, on the one hand, and the crystallite size and photoluminescence intensity, on the other hand. It is shown that the maximum photocatalytic activity is achieved simultaneously with the maximum crystallite size along the 002 direction and the minimum photoluminescence intensity at NaOH concentration during synthesis in the range of 0.4–0.7 M.

METHODS

ZnO nanopowders were obtained by a low-cost chemical precipitation method from a distilled water solution containing zinc acetate dihydrate $(CH_3COO)_2Zn \times 2H_2O$ and sodium hydroxide NaOH. For all solutions the concentration of zinc acetate ($ZnAc_2$) was 0.1 M. Initially, the zinc precursor and the alkali were dissolved in water separately for 30 min. To precipitate zinc oxide nanoparticles (ZnO NPs), sodium hydroxide solution at room temperature was added dropwise to a glass containing the zinc acetate solution, afterwards the entire solution was thoroughly mixed with a magnetic stirrer for 15 min at room temperature. The resulting precipitate was thoroughly washed with distilled water, separated by centrifugation, and then dried in an oven at 100°C for 12 h. The obtained ZnO powders were annealed in a muffle furnace at a temperature of 450°C for 1 h. We prepared several samples by starting from different initial alkali concentration, namely from 0.14 to 2 M NaOH. In the following we discuss the structure, morphology and photocatalytic properties of all obtained samples, named as follows: ZP 20 (0.14 M), ZP 15 (0.27 M), ZP 19 (0.4 M), ZP 22 (0.53 M), ZP 26 (0.7 M), and ZP 23 (1.06 M).

To study the photocatalytic degradation of the RhB dye in the presence of the ZnO NPs under ultraviolet irradiation, 9 mg of each ZnO sample was added to an aqueous solution containing 0.16 mg of RhB per 1 L of distilled water. The solution was treated in an ultrasonic bath for 30 min, followed by stirring with a magnetic stirrer at room temperature. Ultraviolet illumination was provided by a mercury arc lamp (LEH Germany UL Q 14 4P SE) with a power of 14 W. The mercury lamp was located in a flask with the prepared dye solutions.

RESULTS AND DISCUSSION

Sample Morphology

The morphology of the synthesized samples was studied by means of an electronic scanning microscope (SEM) with a direct-filament tungsten cathode (FEI Company) Quanta 200i 3D. **Figure 1** shows the morphology of the ZnO particles

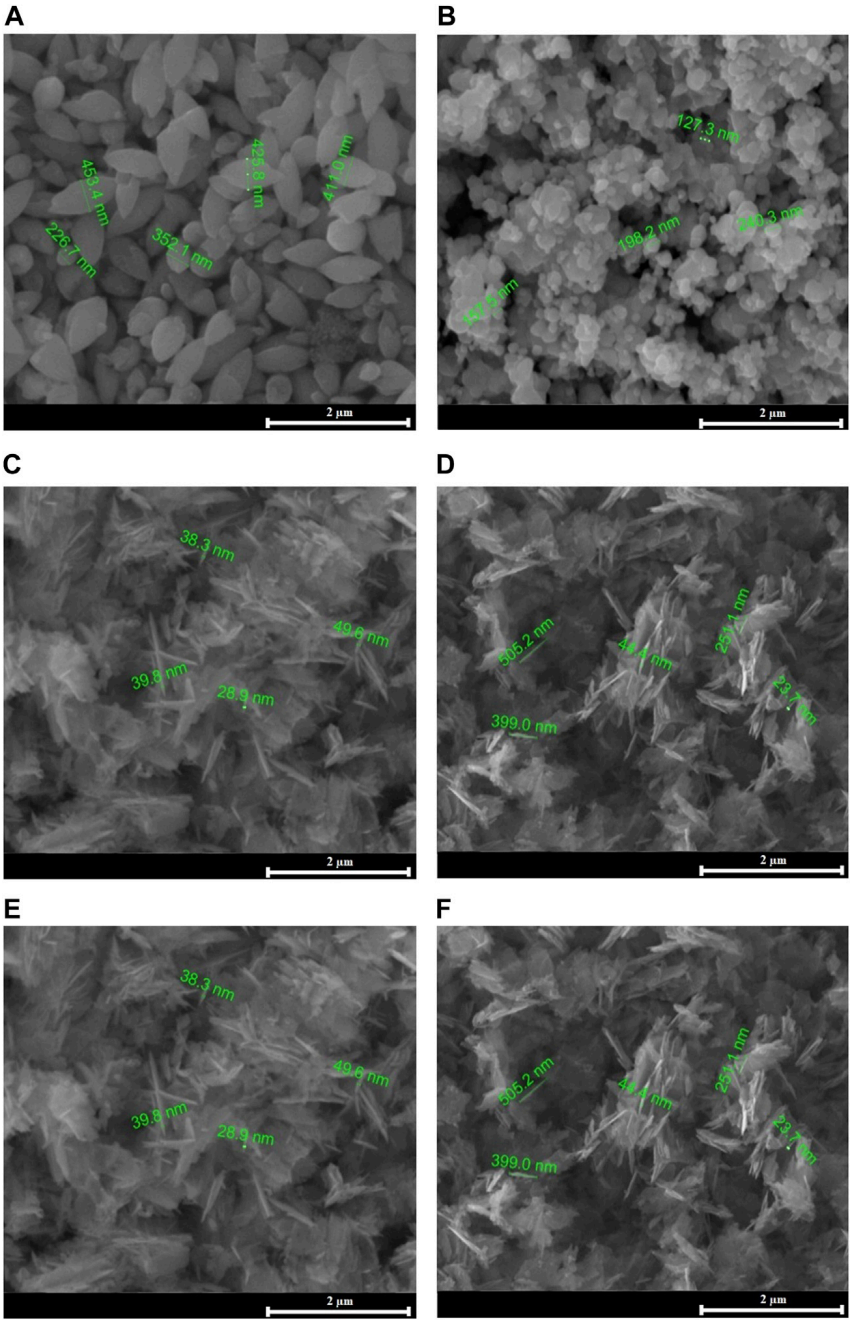

FIGURE 1 | SEM images of the ZnO samples: **(A)**—ZP 20, **(B)**—ZP 15, **(C)**—ZP 19, **(D)**—ZP 22, **(E)**—ZP 26, **(F)**—ZP 23.

obtained at various starting NaOH concentration. An analysis of the SEM images highlights that an increase NaOH concentration in the growth solution (keeping all other synthesis parameters unchanged) leads to a decrease in the geometric parameters (diameter and length) of the synthesized ZnO particles (**Table 1**). In particular, at NaOH concentration of 0.14 M, large pointed elongated particles form (**Figure 1A**) while at a concentration of 0.27 M smaller particles of irregular spherical shape (**Figure 1B**) appear. At (0.4–0.7) M ZnO grows in the form of thin 2D plates (**Figures 1C–E**). An increase in the alkali concentration of the growth solution makes it possible to obtain thinner 2D ZnO structures, but at higher NaOH concentration, the ZnO particles tend to coalesce (see **Figure 1F**).

Transmission electron microscopy (TEM) images were obtained with a JEM-2100 transmission electron microscope operating at an acceleration voltage of 200 kV (**Figure 2**). Results of TEM analysis of ZP 15 and ZP19 samples with different morphology correspond to SEM images (**Figures 1B,C**).

Table 1 shows that an increase of the sodium hydroxide concentration in the growing solution up to 0.4 M leads to a

TABLE 1 | Physicochemical characteristics of the samples.

Sample	FESEM		Aspect ratio, l/d	Cell parameters, Å		Band gap, eV
	Thickness d, nm	Length l, nm		a	c	
ZP 20, 0.14 M NaOH	315 ± 20	1000 ± 20	3.2	3.252	5.213	3.1
ZP 15, 0.27 M NaOH	120 ± 5	400 ± 5	3.3	3.252	5.211	3.05
ZP 19, 0.4 M NaOH	32 ± 5	1000 ± 5	31.25	3.253	5.209	2.95
ZP 22, 0.53 M NaOH	33 ± 5	800 ± 5	23.5	3.251	5.207	2.9
ZP 26, 0.7 M NaOH	33 ± 5	605 ± 5	18.3	3.251	5.208	2.82
ZP 23, 1.06 M NaOH	80 ± 5	250 ± 10	3.1	3.252	5.213	3.07

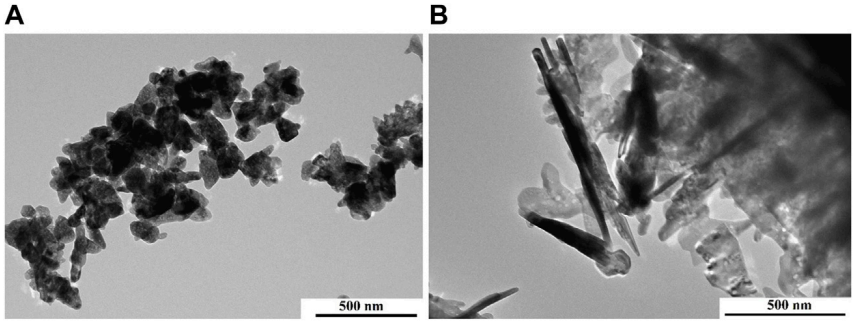

FIGURE 2 | TEM images of the ZnO samples: **(A)**—ZP 15, **(B)**—ZP 19.

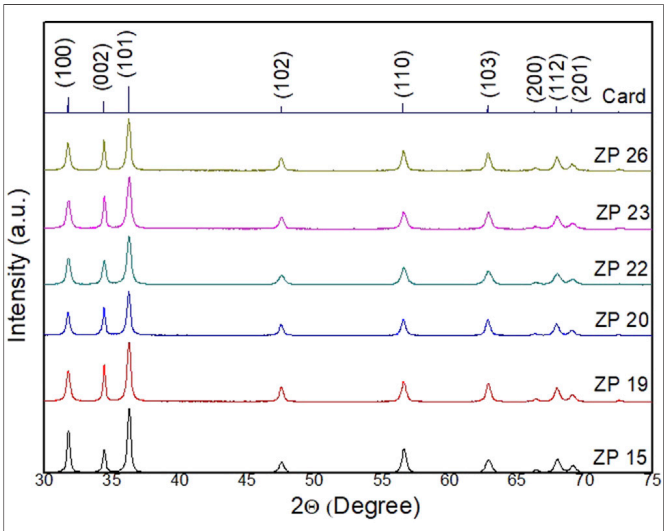

FIGURE 3 | XRD spectra of all synthesized ZnO samples.

gradual increase on the ZnO NP aspect ratio (AR) but with a further increase of the NaOH concentration the AR decreases. The ZP 19 sample has the highest AR.

Phase Studies

XRD measurements were performed on an X-ray diffractometer X'pert MPD PRO (PANalitical) under the same conditions for all samples. The XRD peaks have been labelled according to the reference spectra (JCPDS Card No. 80-0075) of wurtzite ZnO structure (**Figure 3**).

Among all the observed diffraction peaks, the (101) reflex is particularly intense (**Figure 3**) that demonstrates the crystalline nature of the nanoplatelets. A high degree of ordering along (101) direction in comparison with the intensity of other peaks has a significant effect on aspect ratio of particles (Zak et al., 2013). All synthesized samples of the considered series show a slight difference in the intensity and width of the diffraction peaks.

The ZnO crystallites sizes (D) were estimated based on the XRD analysis for the most intense peak (101) by employing the Scherrer's formula,

$$D = k\lambda/\beta cos\theta \quad (1)$$

here k = 0.89 is a dimensionless coefficient (Scherrer's constant), λ = 1.54 Å is the wavelength of CuKa radiation, θ is the diffraction angle, and β is the width of the peak at half-height in radians. The values obtained in this way are consistent with the electron microscopy observation. The evaluating results of the crystal lattice parameters of the samples using Williamson—Hall method (Mote et al., 2012) are shown in **Table 1**. All the studied ZnO samples show a hexagonal wurtzite structure with P63mc space group (Kumaresan et al., 2017) and good crystalline quality, since all diffraction reflexes are very close to the reference sample peaks and correspondingly also the estimated lattice parameters (JCPDS Card No. 80-0075, a—3.2539 Å and c—5.2098 Å).

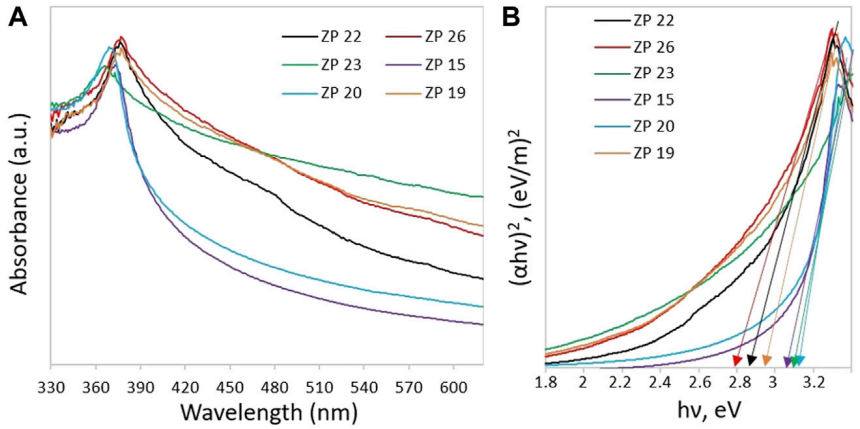

FIGURE 4 | (A) UV–Visible spectra and **(B)** Tauc's plot for the determination of the ZnO samples band gap.

Absorbance Spectra

The optical characteristics of the materials is particularly relevant since it allows predicting the possible photocatalytic behavior of the samples under UV/Vis illumination. The optical absorption spectra of all studied samples, measured with a two-beam UV/Vis Lambda 35 spectrophotometer (PerkinElmer), are shown in **Figure 4A**.

All ZnO NP samples are transparent in the visible region of the electromagnetic spectrum and absorb light in the UV range. **Figure 4B** shows the Tauc's graphs which can be used to identify the samples absorption edge and thus evaluate the optical band gap (E_g) using the following equation:

$$(\alpha h\nu) = A(h\nu - Eg)^n \quad (2)$$

here α is the absorption coefficient; hν is the photon energy; A is a proportionality coefficient; n = 0.5, since ZnO refers to direct bandgap semiconductor material (Rusdi et al., 2011). The equation for the proportionality coefficient A has the form

$$A = \alpha d = -\ln T \quad (3)$$

Here d is the thickness of the film; T is the transmittance coefficient. The plot of value $(\alpha h\nu)^2$ against energy hν allows calculating the value of band gap E_g by extrapolating the linear part of the curve to the horizontal axis. According to **Figure 4B**, the width of the optical band gap of the samples is in the range of 2.82–3.1 eV. The estimated band gap values for all ZnO NP samples are summarized in **Table 1**. In all cases, the actual gap value turned out to be smaller than the reference ZnO value of 3.37 eV (Huang et al., 2015). In particular, the smallest value was found for the ZP 26 sample (~2.82 eV) while the largest for the ZP 20 sample (~3.1 eV). The relationship between the E_g value and the photocatalysis efficiency was discussed in (Ong et al., 2018) and shown in (Di Mauro et al., 2017; EL-Dafrawy et al., 2021; Ramírez et al., 2021).

Photocatalytic Activity

The photocatalytic activity of our ZnO samples was studied by verifying the degradation of a test organic molecule, namely the rhodamine-B (RhB) dye. Upon UV optical excitation of the ZnO nanoparticles, electron-hole (e^-—h^+) pairs are formed, which,

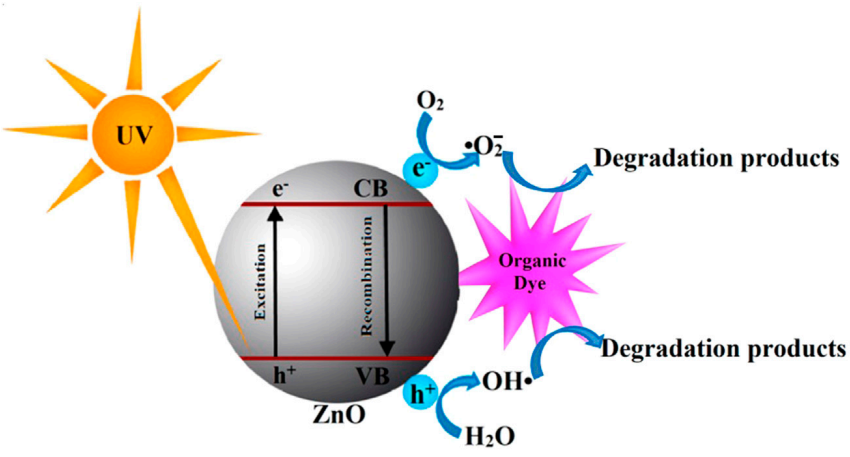

FIGURE 5 | Diagram of the RhB decomposition mechanism on the ZnO NPs surface.

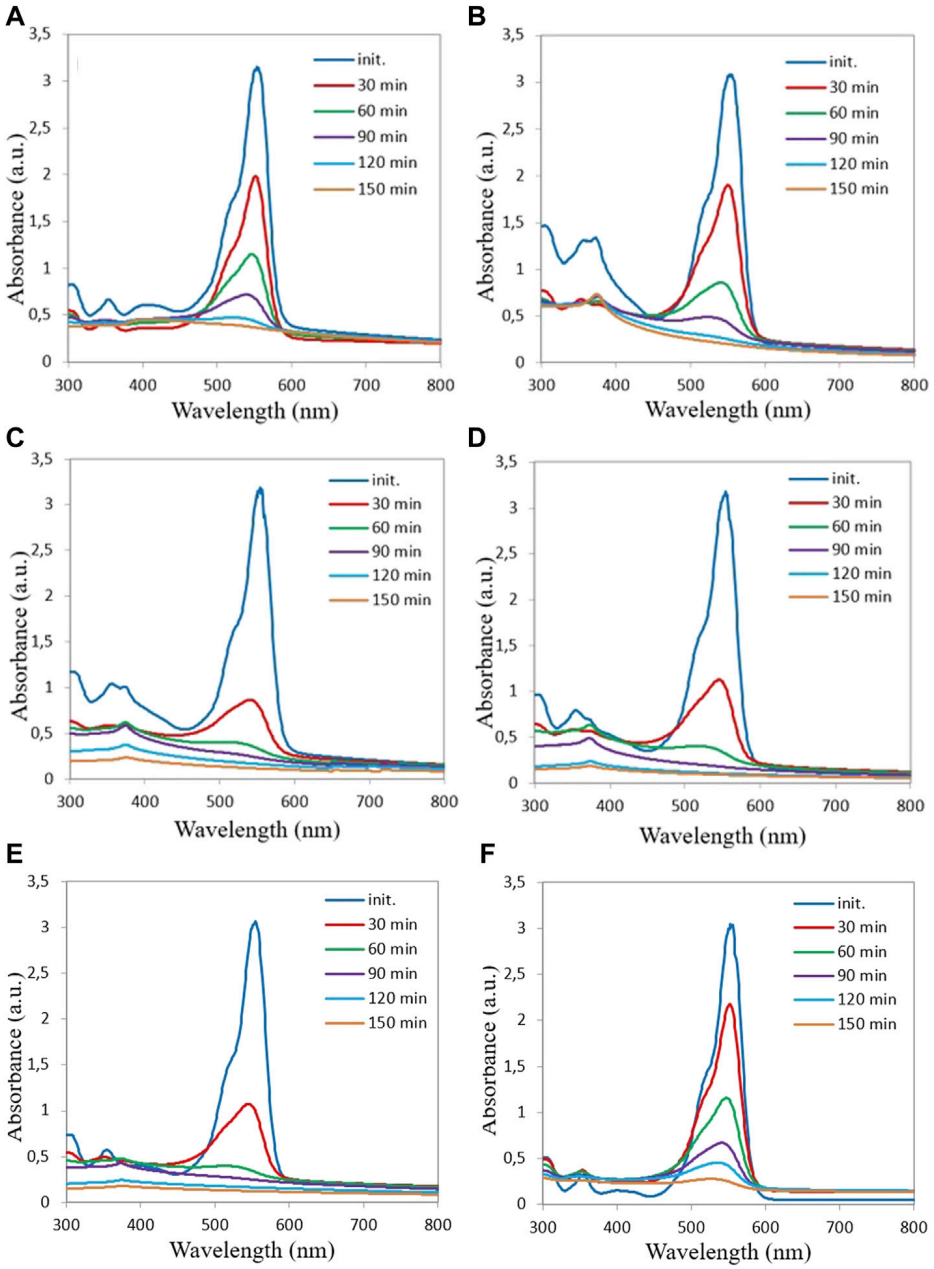

FIGURE 6 | Optical absorption spectra of RhB solutions mixed with different ZnO samples **(A)** ZP 20, **(B)** ZP 15, **(C)** ZP 19, **(D)** ZP 22, **(E)** ZP 26, **(F)** ZP 23 at increasing UV exposure time.

due to the large surface/volume ratio, are easily transferred to the NP surface inducing the rhodamine-B degradation (Ruellas et al., 2019; Azfar et al., 2020; Blažeka et al., 2020). According to the literature [see e.g., (Ong et al., 2018; Khiavi et al., 2019; Nguyen and Nguyen, 2020)], the photocatalytic degradation mechanism can be summarized as follows: absorption of a UV photon excites an electron to the NP conduction band (CB); the electron, e^-, moves to the surface of ZnO NP and it is transferred to an oxygen molecule dissolved in the rhodamine containing solution; the oxygen molecule, O_2, is transformed into a superoxide anion $\bullet O_2^-$, and subsequently, after capturing a proton from the solution it generates a HOO• radicals. At the same time the hole, h^+, generated in the NP valence band (VB) moves to the NP surface reacting either with a water molecule or with a hydroxide (OH^-) originating a reactive OH• species. Hydroxyl radicals and superoxide anions, being the most powerful oxidizing intermediates, cause decomposition of RhB molecules adsorbed on the surface of ZnO NPs. Thus, the negatively charged surface of ZnO promotes the release of holes, which decompose organic matter without an intermediate step. These intermediates are eventually converted into CO_2, H_2O and mineral acids, as summarized in **Figure 5**.

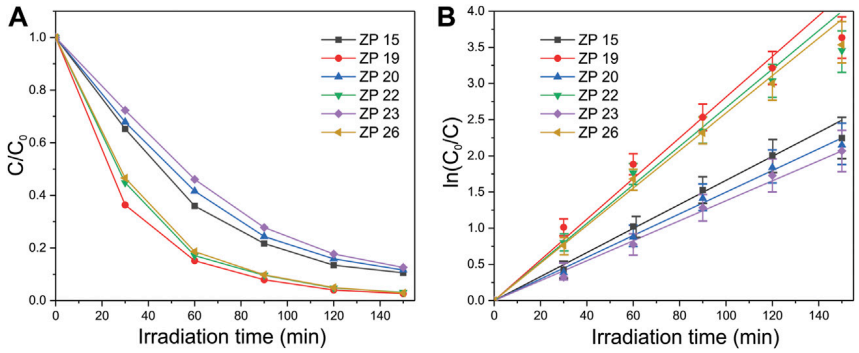

FIGURE 7 | Plots of **(A)** C/C_0 and **(B)** ln (C_0/C) as function of UV light irradiation time for the degradation of RhB dye in the presence of ZnO samples as photocatalyst.

TABLE 2 | Photocatalytic efficiency of the ZnO samples.

Sample	R* after 150 min, %	k, min^{-1}		k_{av}, min^{-1}	k_{av}, hr^{-1}
		min	max		
ZP 20, 0.14 M NaOH	88.36	0.013	0.016	0.015	0.875
ZP 15, 0.27 M NaOH	89.42	0.014	0.017	0.016	0.959
ZP 19, 0.4 M NaOH	97.36	0.024	0.034	0.029	1.731
ZP 22, 0.53 M NaOH	96.85	0.023	0.029	0.026	1.566
ZP 26, 0.7 M NaOH	97.08	0.024	0.028	0.026	1.533
ZP 23, 1.06 M NaOH	87.36	0.011	0.014	0.013	0.794

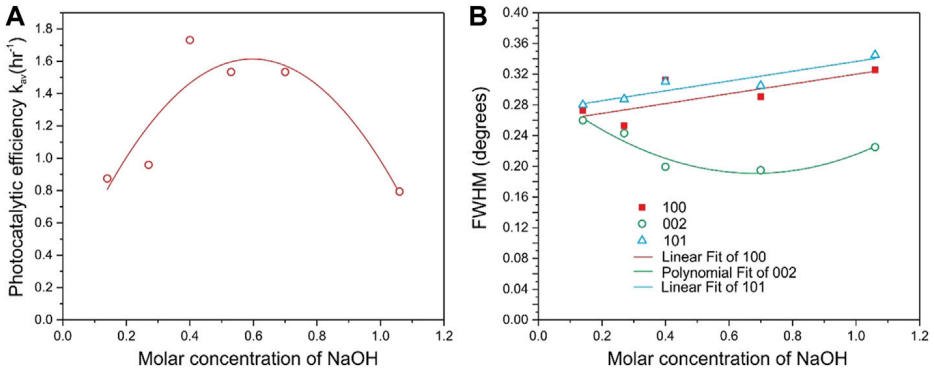

FIGURE 8 | Photocatalytic activity **(A)** and half-width of X-ray reflections 100, 002, and 101 **(B)** of the synthesized samples depending on the molar concentration of NaOH in the growth solution.

Figure 6 shows the degradation spectra of the aqueous RhB solution containing the different ZnO samples described in the previous sections. As it is apparent from an analysis of **Figure 6** the maximum absorption intensity of the initial RhB solution with ZnO powder occurs at 554 nm.

With increasing exposure time, the intensity of the RhB absorption gradually decreases in the presence of the ZnO NPs, which indicates a decrease in the concentration of RhB dye as time proceeds. The relative concentration of the RhB dye decreases with increasing exposure time, which implies that, for all our ZnO samples, the RhB dye significantly degrades on the ZnO NP surfaces under the influence of UV illumination, already after 30 min of exposure.

It is noted that with an increase in the alkali concentration in the growth solution from 0.14 M (ZP 20, **Figure 6A**) up to 0.4 M (ZP 19, **Figure 6C**), the photocatalytic activity of the ZnO samples increases, with a further increase in the NaOH concentration, the photoactivity decreases (ZP 23, **Figure 6F**).

To quantitative analysis the photocatalytic activity of the different ZnO samples, we calculated the ratio $R = C/C_0$ at a function of exposure time (see **Figure 7A**), where C is the dye concentration after irradiation with UV light at maximum

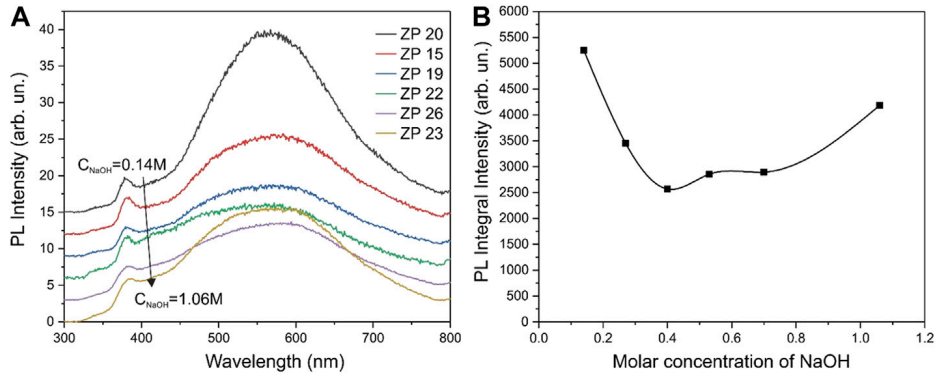

FIGURE 9 | PL spectra of the synthesized ZnO samples taken at room temperature with excitation at a wavelength of 300 nm **(A)** and the dependence of the integrated PL for the same samples on the molar concentration of NaOH in the growth solution **(B)**.

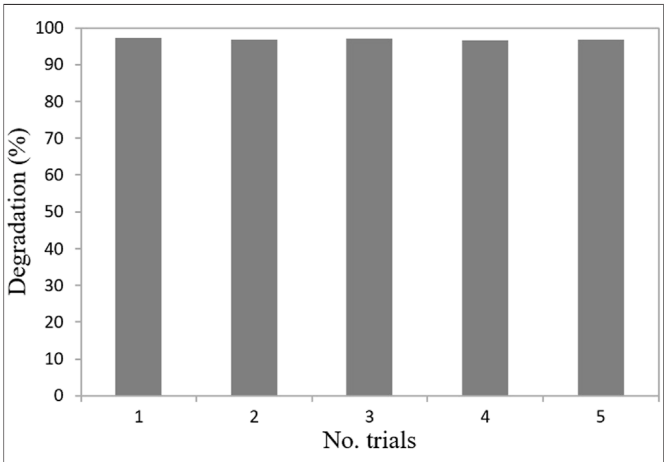

FIGURE 10 | Reuse activity of ZP 19 for RhB dye photodegradation.

absorbance intensity (554 nm), while C_0 is the initial dye concentration. The value of the photodegradation rate k of the ZnO NPs was estimated using the kinetic model proposed by Langmuir–Hinshelwood (Di Mauro et al., 2017; Magalhães et al., 2017; Godin et al., 2018), according to which:

$$\ln(C/C_0) = -kt \quad (4)$$

Hence

$$k = \frac{lnR}{-t} = \frac{ln\,(C_0/C)}{t} \quad (5)$$

The dependence of ln (C_0/C) as a function of the exposure time is shown in **Figure 7B**. The results of the photocatalytic efficiency of the synthesized samples with respect to RhB degradation, including the minimum k_{min}, maximum k_{max} after 30, 60, 90, 120, and 150 min and the average rate k_{av} of dye degradation are shown in **Table 2**. Value k_{av} characterizes an angle of the linear curves slope in **Figure 7B**. It is usualy k_{max} was observed after first 30 min of irradiation, minimal photodegradation rate k_{min} was noted after 150 min of exposure. The percentage of the degraded dye in an aqueous solution for 150 min of illumination in the presence of ZnO NPs is estimated from the ratio R* = 100 (1-R).

From an analysis of **Figures 7A,B** and from the data reported in **Table 2**, it can be noticed that the photocatalytic activity of ZP 19, ZP 22, ZP 26 samples is higher than that of ZP 15, ZP 20, ZP 23 samples. The dependence of the photocatalytic activity of the synthesized samples on the NaOH molar concentration during synthesis is nonmonotonic, as shown in **Figure 8A**.

The XRD and PL data have been analyzed to determine the possible reasons for this non-monotonic relationship. The width of the XRD line of the most intense reflections 100, 002, and 101 depending on the molar concentration of NaOH in the growth solution are shown in **Figure 8B**. **Figure 9A** shows the PL spectra for the obtained ZnO samples, and **Figure 9B** shows the dependence of the integrated PL for the same samples on the molar concentration of NaOH. It can be seen that the XRD data for the 002 reflections (**Figure 8B**) and the integral PL intensity (**Figure 9B**) have nonmonotonic dependences on the NaOH molar concentration and correlate well with the data on photocatalytic activity (**Figure 8A**).

The correlation of the photocatalytic activity of the samples with the XRD and PL data needs to be discussed. As can be seen from **Figure 8A**, the half-width of the 100 and 101 reflections increases monotonically with an increase in the NaOH molar concentration, i.e., the crystallite sizes along the corresponding crystallographic directions decrease. On the other hand, there is a correlation between the half-width of the 002 reflection (**Figure 8B**) and photocatalytic activity (**Figure 8A**), and the maximum photocatalytic activity is reached at the maximum particle size along the 002 direction.

Estimates of the particle sizes along 100 and 101 using the Scherrer formula give a value of 31 ± 2 nm at a NaOH concentration of 0.14 M, and the particle sizes decrease linearly with increasing NaOH concentration to 25 ± 2 nm at a concentration of 1 M. A similar estimate using the Scherrer formula shows that the particle size along 002 nonmonotonically depends on the concentration of NaOH, the average particle size along 002 crystallographic direction reaches a maximum of 42 ± 2 nm at concentrations of 0.4–0.7 M (**Figure 8A**). The data on the

morphology of the samples shown in **Figures 1**, **2** also indicate that rods and plates of ZnO nanocrystals mainly grow at a growth solution concentration of 0.4–0.7 M NaOH.

At the same concentrations, the maximum photocatalytic activity is reached (**Figure 8B**) so it can be concluded that both the size of the particles and their shape, which provides a high specific surface area, have an important influence on the photocatalytic activity. Since the particle sizes along the crystallographic direction 002 reach a maximum at concentrations of 0.4–0.7 M, i.e., growth in this direction is very favorable, one can expect a low concentration of defects in the volume and on the surface of the synthesized samples.

The PL spectra also agree with this conclusion. As shown in **Figure 9**, PL intensity of the radiative recombination through deep defect states in samples obtained at NaOH concentrations in the growth solution of 0.4–0.7 M reaches a minimum value. These results may indicate a reduced concentration of defects in the volume and surface of ZnO nanocrystals in such samples. That is, the intensity of radiative recombination is minimal in the samples due to the low concentration of defects. These results unambiguously indicate that the concentration of defects in the volume and surface of ZnO nanocrystals is low, and, accordingly, the photogenerated free-carrier lifetime is long in such samples. It is the factor of the long lifetime of nonequilibrium carriers that can be the main reason for the high photocatalytic activity of ZnO samples. To concretize the possible photocatalytic mechanism of ZnO nanoparticles, it is necessary to carry out experiments on the analysis of the active species capture, similarly to (Xu et al., 2022). Such work is planned for the next stage of our research.

Reusability

One of the advantages of photocatalysis is the reusability of the catalyst (Pirhashemi et al., 2018). In this work, experiments were carried out to verify the possibility of multiple use of the ZnO NPs as photocatalysts. To check ZnO reusability, the photocatalytic activity of the ZP 19 sample was tested five times. The irradiation time for each test was 150 min. After each rhodamine-B degradation test, the solution was centrifuged to separate the ZnO NPs, that were then added to a new fresh dye solution. The initial dye concentration was the same for all tests.

Figure 10 shows that the photocatalytic activity of ZP 19 sample remained almost unchanged after five cycles. These results confirm that ZP 19 photocatalyst has good recyclability properties.

CONCLUSION

A simple environmentally friendly chemical precipitation method of photocatalytically active ZnO NPs from an aqueous alkaline solution (NaOH) containing zinc acetate at room temperature has been developed. Subsequent heat treatment was used to improve the crystalline quality of the precipitates. The influence of the NaOH concentration on the morphology, structural, optical and photocatalytic properties of the synthesized samples was studied. All studied ZnO samples demonstrate hexagonal wurtzite structure. It is shown that the change in the concentration of alkali in the initial growth solution significantly effects the morphology and aspect ratio of ZnO NPs. The study of the influence of the alkali concentration on the photocatalytic activity of the synthesized ZnO NPs with respect to the degradation of the rhodamine-B organic dye in aqueous solution under the UV radiation showed that RhB decomposes by approximately 97.36% in 150 min in the presence of ZnO samples synthesized from a solution with an alkali concentration of (0.4–0.7) M, having the highest AR value of 31.25–18.3, respectively.

The highest rate of dye degradation ~0.03 min^{-1} during the first 30 min of exposure was recorded for samples synthesized at an alkali growth solution concentration of 0.4–0.7 M.

It is shown that zinc oxide samples with the highest photocatalytic activity also demonstrate the maximum crystallite size along the 002 direction and the minimum photoluminescence intensity through deep levels.

Therefore, the main factors that contribute to high photocatalytic activity are the high specific area of the samples and the low concentration of defects.

Thus, the proposed method of synthesis of ZnO NPs is simple, economical, does not require complex expensive equipment, heating or calcination. It is suitable for large scale production of high active ZnO photocatalysts for the decomposition of organic pollutants under UV radiation due to its simplicity, low cost, high productivity, recyclability and excellent product characteristics.

DATA AVAILABILITY STATEMENT

The original contributions presented in the study are included in the article/Supplementary Material, further inquiries can be directed to the corresponding author.

AUTHOR CONTRIBUTIONS

Conception and design of study: YK, GB, LG, GC and KA; acquisition of data: YK, GB, LG, GC and KA; analysis and/or interpretation of data: YK, GB, LG, GC and KA. Drafting the manuscript: YK, LG, GC and KA; revising the manuscript critically for important intellectual content: YK, LG, GC and KA. Approval of the version of the manuscript to be published: YK, GB, LG, GC and KA.

FUNDING

This research has been funded by the Science Committee of the Ministry of Education and Science of the Republic of Kazakhstan (Grant No. AP08856173).

REFERENCES

Adam, R. E., Pozina, G., Willander, M., and Nur, O. (2018). Synthesis of ZnO Nanoparticles by Co–precipitation Method for Solar Driven Photodegradation of Congo Red Dye at Different pH. *Photon. Nanostructures – Fundamentals Appl.* 32, 11–18. doi:10.1016/j.photonics.2018.08.005

Ahmoum, H., Li, G., Belakry, S., Boughrara, M., Su'ait, M. S., Kerouad, M., et al. (2021). Structural, Morphological and Transport Properties of Ni Doped ZnO Thin Films Deposited by thermal Co-evaporation Method. *Mater. Sci. Semiconductor Process.* 123, 105530. doi:10.1016/j.mssp.2020.105530

Aljaafari, A. (2020). Size Dependent Photocatalytic Activity of ZnO Nanosheets for Degradation of Methyl Red. *Front. Mater.* 7, 562693. doi:10.3389/fmats.2020.562693

Alshamsi, H. A. H., and Hussein, B. S. (2018). Hydrothermal Preparation of Silver Doping Zinc Oxide Nanoparticles: Study the Characterization and Photocatalytic Activity. *Oriental J. Chem.* 34, 1898–1907. doi:10.13005/ojc/3404025

Al–Namshah, K. S. (2021). Impact of CuO Incorporation on the Photocatalytic Enhancement of the Mesostructured Fe_2O_3 Nanocomposite. *Appl. Nanoscience* 11, 467–476. doi:10.1007/s13204-020-01605-6

Azfar, A. K., Kasim, M. F., Lokman, I. M., Rafaie, H. A., and Mastuli, M. S. (2020). Comparative Study on Photocatalytic Activity of Transition Metals (Ag and Ni)-Doped ZnO Nanomaterials Synthesized via Sol-Gel Method. *R. Soc. Open Sci.* 7, 191590. doi:10.1098/rsos.191590

Blažeka, D., Car, J., Klobučar, N., Jurov, A., Zavašnik, J., Jagodar, A., et al. (2020). Photodegradation of Methylene Blue and Rhodamine B Using Laser-Synthesized ZnO Nanoparticles. *Materials* 13, 4357. doi:10.3390/ma13194357

Cao, Y.-Q., Zi, T.-Q., Zhao, X.-R., Liu, C., Ren, Q., Fang, J.-B., et al. (2020). Enhanced Visible Light Photocatalytic Activity of Fe2O3 Modified TiO2 Prepared by Atomic Layer Deposition. *Sci. Rep.* 10, 13437. doi:10.1038/s41598-020-70352-z

Consonni, V., Briscoe, J., Kärber, E., Li, X., and Cossuet, T. (2019). ZnO Nanowires for Solar Cells: a Comprehensive Review. *Nanotechnology* 30, 362001. doi:10.1088/1361–6528/ab1f2e

Di Mauro, A., Fragalà, M. E., Privitera, V., and Impellizzeri, G. (2017). ZnO for Application in Photocatalysis: From Thin Films to Nanostructures. *Mater. Sci. Semiconductor Process.* 69, 44–51. doi:10.1016/j.mssp.2017.03.029

El-Dafrawy, S. M., Tarek, M., Samra, S., and Hassan, S. M. (2021). Synthesis, Photocatalytic and Antidiabetic Properties of ZnO/PVA Nanoparticles. *Sci. Rep.* 11, 11404. doi:10.1038/s41598-021-90846-8

Ferreira, S. H., Morais, M., Nunes, D., Oliveira, M. J., Rovisco, A., Pimentel, A., et al. (2021). High UV and Sunlight Photocatalytic Performance of Porous ZnO Nanostructures Synthesized by a Facile and Fast Microwave Hydrothermal Method. *Materials* 14, 2385. doi:10.3390/ma14092385

Godin, R., Hisatomi, T., Domen, K., and Durrant, J. R. (2018). Understanding the Visible–Light Photocatalytic Activity of GaN:ZnO Solid Solution: the Role of $Rh_{2-y}Cr_yO_3$ Cocatalyst and Charge Carrier Lifetimes over Tens of Seconds. *Chem. Sci.* 9, 7546–7555. doi:10.1039/C8SC02348D

Hamid, N., Suhaimi, S., Othman, M. Z., and Ismail, W. Z. W. (2021). A Review on Thermal Evaporation Method to Synthesis Zinc Oxide as Photocatalytic Material. *Nano Hybrids and Composites* 31, 55–63. doi:10.4028/www.scientific.net/NHC.31.55

Haque, M. J., Bellah, M. M., Hassan, M. R., and Rahman, S. (2020). Synthesis of ZnO Nanoparticles by Two Different Methods & Comparison of Their Structural, Antibacterial, Photocatalytic and Optical Properties. *Nano Ex.* 1, 010007. doi:10.1088/2632-959x/ab7a43

Harun, K., Hussain, F., Purwanto, A., Sahraoui, B., Zawadzka, A., and Mohamad, A. A. (2017). Sol–gel Synthesized ZnO for Optoelectronics Applications: a Characterization Review. *Mater. Res. Express* 4, 122001. doi:10.1088/2053–1591/aa9e82

Hodges, B. C., Cates, E. L., and Kim, J.-H. (2018). Challenges and Prospects of Advanced Oxidation Water Treatment Processes Using Catalytic Nanomaterials. *Nat. Nanotech* 13, 642–650. doi:10.1038/s41565-018-0216-x

Huang, N., Shu, J., Wang, Z., Chen, M., Ren, C., and Zhang, W. (2015). One-step Pyrolytic Synthesis of ZnO Nanorods with Enhanced Photocatalytic Activity and High Photostability under Visible Light and UV Light Irradiation. *J. Alloys Compd.* 648, 919–929. doi:10.1016/j.jallcom.2015.07.039

Islam, M. R., and Azam, M. G. (2021). Enhanced Photocatalytic Activity of Mg-Doped ZnO Thin Films Prepared by Sol-Gel Method. *Surf. Eng.* 37, 775–783. doi:10.1080/02670844.2020.1801143

Jeon, T. H., Koo, M. S., Kim, H., and Choi, W. (2018). Dual-functional Photocatalytic and Photoelectrocatalytic Systems for Energy- and Resource-Recovering Water Treatment. *ACS Catal.* 8, 11542–11563. doi:10.1021/acscatal.8b03521

Kang, Y., Yu, F., Zhang, L., Wang, W., Chen, L., and Li, Y. (2021). Review of ZnO–Based Nanomaterials in Gas Sensors. *Solid State Ionics* 360, 115544. doi:10.1016/j.ssi.2020.115544

Katal, R., Masudy-Panah, S., Tanhaei, M., Farahani, M. H. D. A., and Jiangyong, H. (2020). A Review on the Synthesis of the Various Types of Anatase TiO2 Facets and Their Applications for Photocatalysis. *Chem. Eng. J.* 384, 123384. doi:10.1016/j.cej.2019.123384

Khiavi, N. D., Katal, R., Eshkalak, S. K., Masudy–Panah, S., Ramakrishna, S., and Jiangyong, H. (2019). Visible Light Driven Heterojunction Photocatalyst of CuO–Cu_2O Thin Films for Photocatalytic Degradation of Organic Pollutants. *Nanomaterials (Basel)* 9, 1011. doi:10.3390/nano9071011

Khudiar, S. S., Mutlak, F. A.-H., and Nayef, U. M. (2021). Synthesis of ZnO Nanostructures by Hydrothermal Method Deposited on Porous Silicon for Photo-Conversion Application. *Optik* 247, 167903. doi:10.1016/j.ijleo.2021.167903

Kumaresan, N., Ramamurthi, K., Ramesh Babu, R., Sethuraman, K., and Moorthy Babu, S. (2017). Hydrothermally Grown ZnO Nanoparticles for Effective Photocatalytic Activity. *Appl. Surf. Sci.* 418, 138–146. doi:10.1016/j.apsusc.2016.12.231

Liang, S., Sui, G., Li, J., Guo, D., Luo, Z., Xu, R., et al. (2022). ZIF-L-derived Porous C-Doped ZnO/CdS Graded Nanorods with Z-Scheme Heterojunctions for Enhanced Photocatalytic Hydrogen Evolution. *Int. J. Hydrogen Energ.* 47, 11190–11202. in press. doi:10.1016/j.ijhydene.2022.01.154

Magalhães, P., Andrade, L., Nunes, O. C., and Mendes, A. (2017). Titanium Dioxide Photocatalysis: Fundamentals and Application on Photoinactivation. *Rev. Adv. Mater. Sci.* 51, 91–129.

Mirzaeifard, Z., Shariatinia, Z., Jourshabani, M., and Rezaei Darvishi, S. M. (2020). ZnO Photocatalyst Revisited: Effective Photocatalytic Degradation of Emerging Contaminants Using S-Doped ZnO Nanoparticles under Visible Light Radiation. *Ind. Eng. Chem. Res.* 59, 15894–15911. doi:10.1021/acs.iecr.0c03192

Mohan, S., Vellakkat, M., Aravind, A., and U, R. (2020). Hydrothermal Synthesis and Characterization of Zinc Oxide Nanoparticles of Various Shapes under Different Reaction Conditions. *Nano Ex.* 1, 030028. doi:10.1088/2632-959x/abc813

Mote, V., Purushotham, Y., and Dole, B. (2012). Williamson-hall Analysis in Estimation of Lattice Strain in Nanometer-Sized ZnO Particles. *J. Theor. Appl. Phys.* 6, 6. doi:10.1186/2251-7235-6-6

Naji, H. K., Oda, A. M., Abdulaljeleel, W., Abdilkadhim, H., and Hefdhi, R. (2020). ZNO-Ag/PS and ZnO/PS Films for Photocatalytic Degradation of Methylene Blue. *Indones. J. Chem.* 20, 314–323. doi:10.22146/ijc.41347

Nguyen, N. T., and Nguyen, V. A. (2020). Synthesis, Characterization, and Photocatalytic Activity of ZnO Nanomaterials Prepared by a Green, Nonchemical Route. *J. Nanomater.* 2020, 1–8. doi:10.1155/2020/1768371

Ong, C. B., Ng, L. Y., and Mohammad, A. W. (2018). A Review of ZnO Nanoparticles as Solar Photocatalysts: Synthesis, Mechanisms and Applications. *Renew. Sustain. Energ. Rev.* 81, 536–551. doi:10.1016/j.rser.2017.08.020

Otis, G., Ejgenberg, M., and Mastai, Y. (2021). Solvent-Free Mechanochemical Synthesis of ZnO Nanoparticles by High-Energy Ball Milling of ε-Zn(OH)2 Crystals. *Nanomaterials* 11, 238. doi:10.3390/nano11010238

Pirhashemi, M., Habibi-Yangjeh, A., and Rahim Pouran, S. (2018). Review on the Criteria Anticipated for the Fabrication of Highly Efficient ZnO-Based Visible-Light-Driven Photocatalysts. *J. Ind. Eng. Chem.* 62, 1–25. doi:10.1016/j.jiec.2018.01.012

Qi, K., Cheng, B., Yu, J., and Ho, W. (2017). Review on the Improvement of the Photocatalytic and Antibacterial Activities of ZnO. *J. Alloys Compd.* 727, 792–820. doi:10.1016/j.jallcom.2017.08.142

Rahman, F. (2019). Zinc Oxide Light–Emitting Diodes: a Review. *Opt. Eng.* 58, 1010901. doi:10.1117/1.oe.58.1.010901

Ramírez, A. E., Montero-Muñoz, M., López, L. L., Ramos-Ibarra, J. E., Coaquira, J. A. H., Heinrichs, B., et al. (2021). Significantly Enhancement of Sunlight

Photocatalytic Performance of ZnO by Doping with Transition Metal Oxides. *Sci. Rep.* 11, 2804. doi:10.1038/s41598-020-78568–910.1038/s41598-020-78568-9

Ruellas, T. M. O., Domingos, G. H. S., Peçanha, L. O. O., Maestrelli, S. C., and Giraldi, T. R. (2019). Photodegradation of Rhodamine B Catalyzed by ZnO Pellets. *Cerâmica* 65, 47–53. doi:10.1590/0366-6913201965s12609

Rusdi, R., Rahman, A. A., Mohamed, N. S., Kamarudin, N., and Kamarulzaman, N. (2011). Preparation and Band gap Energies of ZnO Nanotubes, Nanorods and Spherical Nanostructures. *Powder Technol.* 210, 18–22. doi:10.1016/j.powtec.2011.02.005

Shanmuganathan, V., Kumar, J. S., Pachaiappan, R., and Thangadurai, P. (2021). Transition Metal Ion–Doped In2O3 Nanocubes: Investigation of Their Photocatalytic Degradation Activity under Sunlight. *Nanoscale Adv.* 3, 471–485. doi:10.1039/D0NA00694G

Shu, Y., Duan, X., Niu, Q., Xie, R., Zhang, P., Pan, Y., et al. (2021). Mechanochemical Alkali-Metal-Salt-Mediated Synthesis of ZnO Nanocrystals with Abundant Oxygen Vacancies: An Efficient Support for Pd-Based Catalyst. *Chem. Eng. J.* 426, 131757. doi:10.1016/j.cej.2021.13175743

Shuai, H., Wang, J., Ren, F., and Du, G. (2021). Preparation of ZnO/Brucite Functional Composite Powder by the Mechanochemical Method. *Front. Mater.* 8, 801003. doi:10.3389/fmats.2021.801003

Sousa, J. C. G., Ribeiro, A. R., Barbosa, M. O., Pereira, M. F. R., and Silva, A. M. T. (2018). A Review on Environmental Monitoring of Water Organic Pollutants Identified by EU Guidelines. *J. Hazard. Mater.* 344, 146–162. doi:10.1016/j.jhazmat.2017.09.058

Su, Y., Li, H., Ma, H., Wang, H., Robertson, J., and Nathan, A. (2018). Dye-Assisted Transformation of Cu2O Nanocrystals to Amorphous CuxO Nanoflakes for Enhanced Photocatalytic Performance. *ACS Omega* 3, 1939–1945. doi:10.1021/acsomega.7b01610.1021/acsomega.7b01612

Tasso Guaraldo, T., Wenk, J., and Mattia, D. (2021). Photocatalytic ZnO Foams for Micropollutant Degradation. *Adv. Sustain. Syst.* 5, 2000208. doi:10.1002/adsu.202000208

Wallace, R., Brown, A. P., Brydson, R., Wegner, K., and Milne, S. J. (2013). Synthesis of ZnO Nanoparticles by Flame spray Pyrolysis and Characterisation Protocol. *J. Mater. Sci.* 48, 6393–6403. doi:10.1007/s10853–013–7439–x

Wang, C–N., Li, Y–L., Gong, F–L., Zhang, Y–H., Fang, S–M., and Zhang, H–L. (2020). Advances in Doped ZnO Nanostructures for Gas Sensor. *Chem. Rec.* 20, 1553–1567. doi:10.1002/tcr.202000088

Wibowo, A., Marsudi, M. A., Amal, M. I., Ananda, M. B., Stephanie, R., Ardy, H., et al. (2020). ZnO Nanostructured Materials for Emerging Solar Cell Applications. *RSC Adv.* 10, 42838–42859. doi:10.1039/D0RA07689A

Widiyandari, H., Wijayanti, S., Prasetio, A., and Purwanto, A. (2020). ZnO Hollow Sphere Prepared by Flame spray Pyrolysis Serves as an Anti-reflection Layer that Improves the Performance of Dye-Sensitized Solar Cells. *Opt. Mater.* 107, 110077. doi:10.1016/j.optmat.2020.110077

Xu, R., Li, J., Sui, G., Zhuang, Y., Guo, D., Luo, Z., et al. (2022). Constructing Supramolecular Self-Assembled Porous G-C3n4 Nanosheets Containing Thiophene-Groups for Excellent Photocatalytic Performance under Visible Light. *Appl. Surf. Sci.* 578, 152064. doi:10.1016/j.apsusc.2021.152064

Zak, A. K., Majid, W. H., Wang, H. Z., Yousefi, R., Golsheikh, A. M., and Ren, Z. F. (2013). Sonochemical Synthesis of Hierarchical ZnO Nanostructures. *Ultrason. Sonochem.* 20, 395–400. doi:10.1016/j.ultsonch.2012.07.001

Zakria, M., Huynh, T. T., Ling, F. C. C., Su, S. C., Phillips, M. R., and Ton-That, C. (2019). Highly Luminescent MgZnO/ZnO Multiple Quantum Wells for Photonics Devices. *ACS Appl. Nano Mater.* 2, 2574–2579. doi:10.1021/acsanm.9b00592

Zhang, T., Liu, J., Zhou, F., Zhou, S., Wu, J., Chen, D., et al. (2020). Polymer-Coated Fe2O3 Nanoparticles for Photocatalytic Degradation of Organic Materials and Antibiotics in Water. *ACS Appl. Nano Mater.* 3, 9200–9208. doi:10.1021/acsanm.0c01829

Conflict of Interest: The authors declare that the research was conducted in the absence of any commercial or financial relationships that could be construed as a potential conflict of interest.

Publisher's Note: All claims expressed in this article are solely those of the authors and do not necessarily represent those of their affiliated organizations, or those of the publisher, the editors and the reviewers. Any product that may be evaluated in this article, or claim that may be made by its manufacturer, is not guaranteed or endorsed by the publisher.